

SIMULATION OF STRUCTURAL TRANSFORMATIONS IN NANOPARTICLES

Peter ENTEL, Magnus KRETH, Ralf MEYER*, Kai KADAU**

Institute of Physics, University of Duisburg–Essen, 47048 Duisburg, Germany

*Département de Physique, Université de Montréal, C.P. 6128, Montréal H3C 3J7, Canada

**Los Alamos National Laboratory, T-11, MS B262, Los Alamos, NM 87545, U.S.A.

Structural changes in solid and liquid like clusters and nanoparticles have been investigated by means of molecular dynamics simulations. While in the solid phases of the clusters the reactions leading to structural changes spontaneously occur upon heating, the reverse transition, when decreasing the temperature, is often hindered because of large undercooling effects and missing nucleation sites. Similar tendencies are observed when melting and freezing the clusters; while melting occurs without overheating, freezing is sterically hindered by the development of false symmetries. Both the austenitic transformation as well as the melting temperature scale with the inverse of the particle diameter.

1. INTRODUCTION

Phase transitions in finite systems like melting and freezing of clusters¹, changes of the crystalline or amorphous structure in nanocrystalline materials² as well as changes of the electronic spectrum of magnetic nanoparticles³ and ferroelectric material at molecular level⁴ and inorganic and organic semiconductors on a molecular scale⁵ are of utmost interest for technological fabrication of functional nanomaterials.

In this contribution we concentrate on the structure and phase transformation of nano-scale Fe–Ni and Al particles. Early experimental investigations of Fe–Ni powder showed a reduction of the martensitic transformation temperature, which was tentatively related to the lack of heterogeneities and other nucleation sites in the small particles⁶. With refinement of experimental techniques even smaller particles could be investigated. For example, Tadaki *et al.* investigated Fe–Ni nanoparticles with a diameter around 6 nm, i.e., particles with some 10^3 atoms². They explained the reduction of the martensitic start temperature, M_S , to be a consequence of the reduced equilibrium temperature T_0 (corresponding to equal free energies of martensite and austenite) with decreasing particle size.

The calculations of the structure of Al, Fe–Ni and other transition–metal nanoparticles show further details. With decreasing particle size the vibrational density of states of the particles (and corresponding nanocrystalline materials) shows additional spectral weight at low frequencies stemming from the vibrations of the atoms in the outer layers of the particles⁷. This goes hand in hand with another observation that nanocrystalline materials

undergo elastic changes when decreasing the average grain size to a few nanometers: The materials first show additional hardening due to accumulation of lattice defects (like dislocations) in the grain boundaries (Hall–Petch effect); when further decreasing the grain sizes the nanocrystalline systems show a crossover to a regime with unusual softening (reverse Hall–Petch effect)^{8,9}. In both cases, the increase as well as the decrease of hardness scale with the inverse square of the particle diameter^{8,9}. Figure 1 shows the Hall–Petch effect for a series of nanophase materials¹⁰.

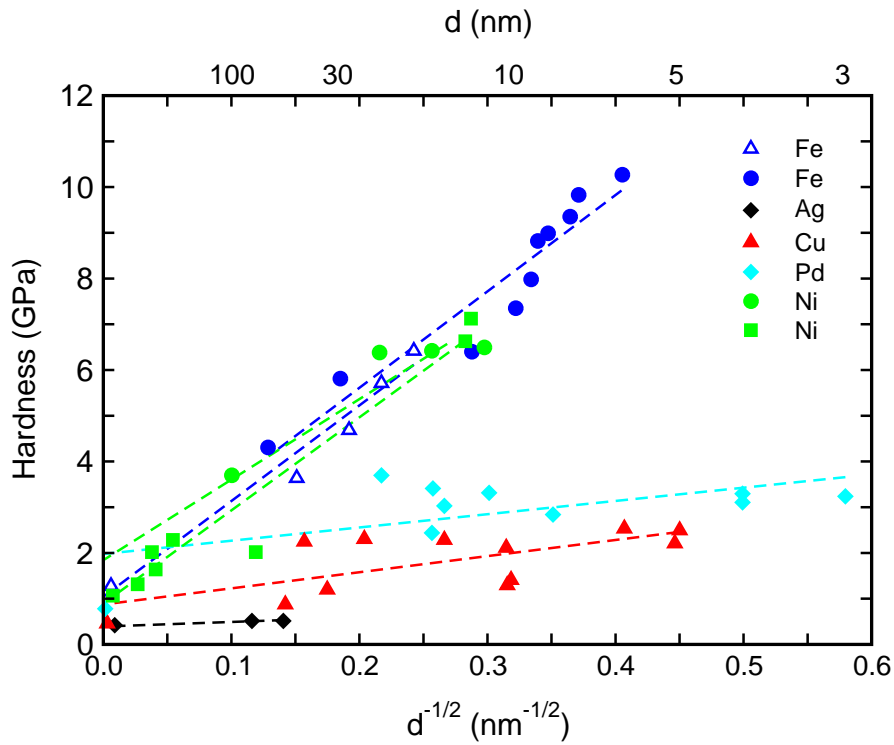


FIGURE 1

Variation of the hardness with $d^{-1/2}$, where d is the average grain diameter, for a selected class of nanophase metals synthesized from gas–condensed clusters compared with their coarse–grained counterparts (values at $d^{-1/2} \rightarrow 0$). Values have been taken from Siegel and Fougere which also gives the references of the original works¹⁰.

The original Hall–Petch relation^{11,12}

$$H_V = \sigma_y + k_y d^{-1/2} \quad (1)$$

(where H_V is the hardness, σ_y the intrinsic stress resisting dislocation motion and k_y is a constant) thus holds for nanomaterials with small enough average grain diameters.

With respect to phase transformation of individual grains or nucleation of structural precursors in the grain boundaries of the nanophase materials we now meet a rather complex situation, since, with decreasing particles sizes and decreasing possibilities of nucleation sites and simultaneous increasing hardness, structural changes as they occur in the corresponding bulk materials may be hindered due to additional energy

barriers. On the other hand, the extra hardness gradually disappears and is replaced by elastically softer grain boundaries for still smaller particle sizes, which will facilitate the nucleation of martensite. This is indeed observed in the molecular dynamics simulations of sintered Fe–Ni nanoparticles at low temperatures¹³. In the following we will discuss a few characteristic features of nucleation and local symmetry changes in Fe–Ni nanoalloys and Al particles.

2. NUCLEATION OF MARTENSITE AND AUSTENITE IN BULK FE–NI ALLOYS

In spite of the diversity of martensitic transformations the martensitic nucleation, i.e., the instability of the high-temperature parent phase of the non-magnetic/magnetic Hume–Rothery and non-Hume-Rothery alloys, is usually related to a critical value of the valence electron number per atom (which is $e/a \approx 1.5$ for the β -phase alloys), for which Fermi–surface nesting induces strong electron–phonon coupling effects and Kohn-like anomalies resulting in a lowering of the electronic energy due to the (in general diffusionless) cooperative displacement of the atoms¹⁴. Note that changes in the structure to maintain a *favorable* valence electron concentration may also be the driving force for the formation of icosahedral quasicrystals (here the critical concentration is $e/a \approx 2.1$)¹⁵. At finite temperatures this electronic *driving force* competes with the high entropy of the parent structure (for example, BCC), which stabilizes the usually less-close packed high-temperature austenitic structure with respect to the more close-packed low-temperature martensitic structure (note that in contrast in the ferrous alloys the low-temperature phase has the less-closed packed structure). In the ferrous alloys, due to the positive volume change at the transition, the origin is believed to be magnetic. The technologically relevant and unique properties of martensites are related to the macroscopic appearance of the shape–memory effect, superelasticity and rubber-like behavior. With respect to nanoscience it is then of interest to see how martensite evolves on the nano-scale, i.e., practically on the atomic level.

To start the discussion we show in Fig. 2 the experimental and theoretical phase diagrams of bulk Fe–Ni alloys over the whole composition range¹⁶. The remarkable fact is that the differences of total energies between the different phases obtained by *ab initio* calculations allow to qualitatively reproduce the trends in the experimental phase diagram. The dots in Fig. 2 mark the results obtained by molecular dynamics simulations on the basis of *embedded atom potentials* for the austenitic transition (upon heating) and the martensitic transition (upon cooling). While the austenitic transition temperatures meet the experimental data, the nucleation of martensite is only poorly reproduced; in order to get the martensitic transformation at all, a large number of defects has to be introduced into the matrix¹⁷. This shows the general difficulty to observe homogeneous nucleation processes in molecular dynamics simulations because of the limited time scale, which is

ps to ns (one has to perform extremely long runs to observe homogeneous nucleation, see, for example the recent successful simulated nucleation of ice in undercooled water¹⁸).

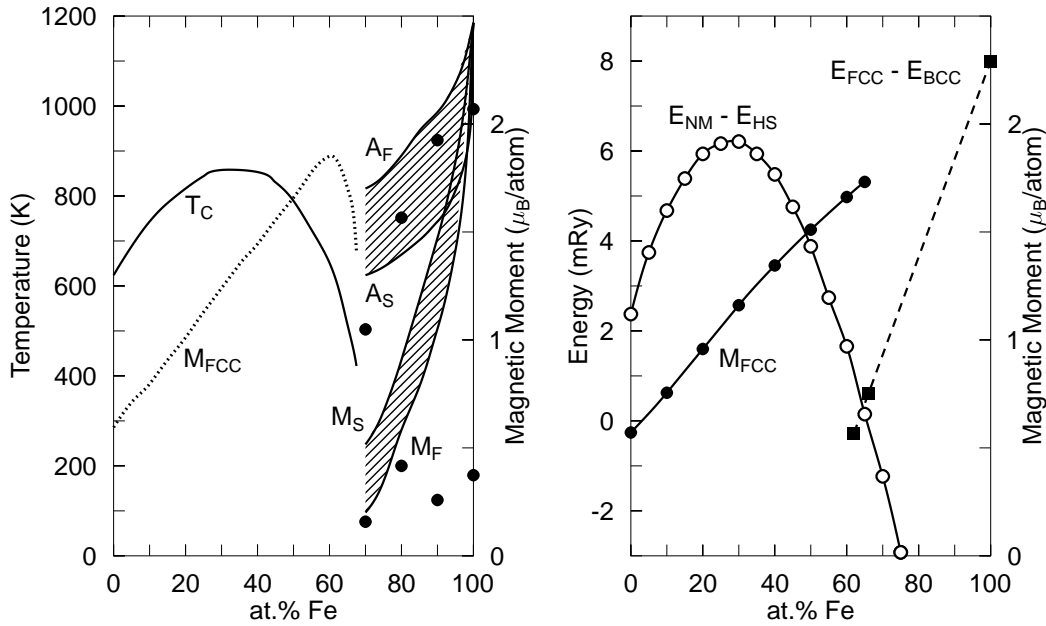


FIGURE 2

The experimental phase diagram (left) shows the Curie temperature T_c and the magnetization M_{FCC} of the alloys in the FCC structure, as well as the austenite and martensite start and final temperatures, $A_{S,F}$ and $M_{S,F}$, respectively, while the dots are results of molecular dynamics simulations. The *theoretical phase diagram* corresponds to *ab initio* total energy differences between the nonmagnetic (NM) and high-spin (HS) phases and the alloys in the FCC and BCC structures¹⁶.

3. NUCLEATION OF MARTENSITE/AUSTENITE IN FE-NI NANOPARTICLES

In general the application of the embedded atom method to Fe and Ni has yielded reasonable results for the structural changes occurring in the bulk material and in thin films^{19,20}. We have used the same embedded atom potentials to study nucleation and structure changes in nanoparticles. Modification of the potentials due to free surfaces of the particles have not been calculated. For the large-scale simulations we used a code developed in our group as well as the SPaSM code developed by the Los Alamos group²¹.

The nucleation of martensite in Fe-Ni nanoparticles and nanophase Fe-Ni has been investigated in conjunction with studies of sintering of Fe-Ni particles^{13,16,22}. In search of the crossover from Hall-Petch to anti Hall-Petch behavior also sintered Al Particles have been studied⁸. The general observation is that the martensitic transformation is usually hindered for the individual particles if they have spherical-like shape and no additional defects. This can nicely be demonstrated by following the heterogeneous martensitic nucleation at a plane defect in an otherwise ideal spherical $Fe_{80}Ni_{20}$ particle²² which is shown in Fig. 3. Note that without the defect the particle does not transform to BCC but

retains its metastable FCC structure.

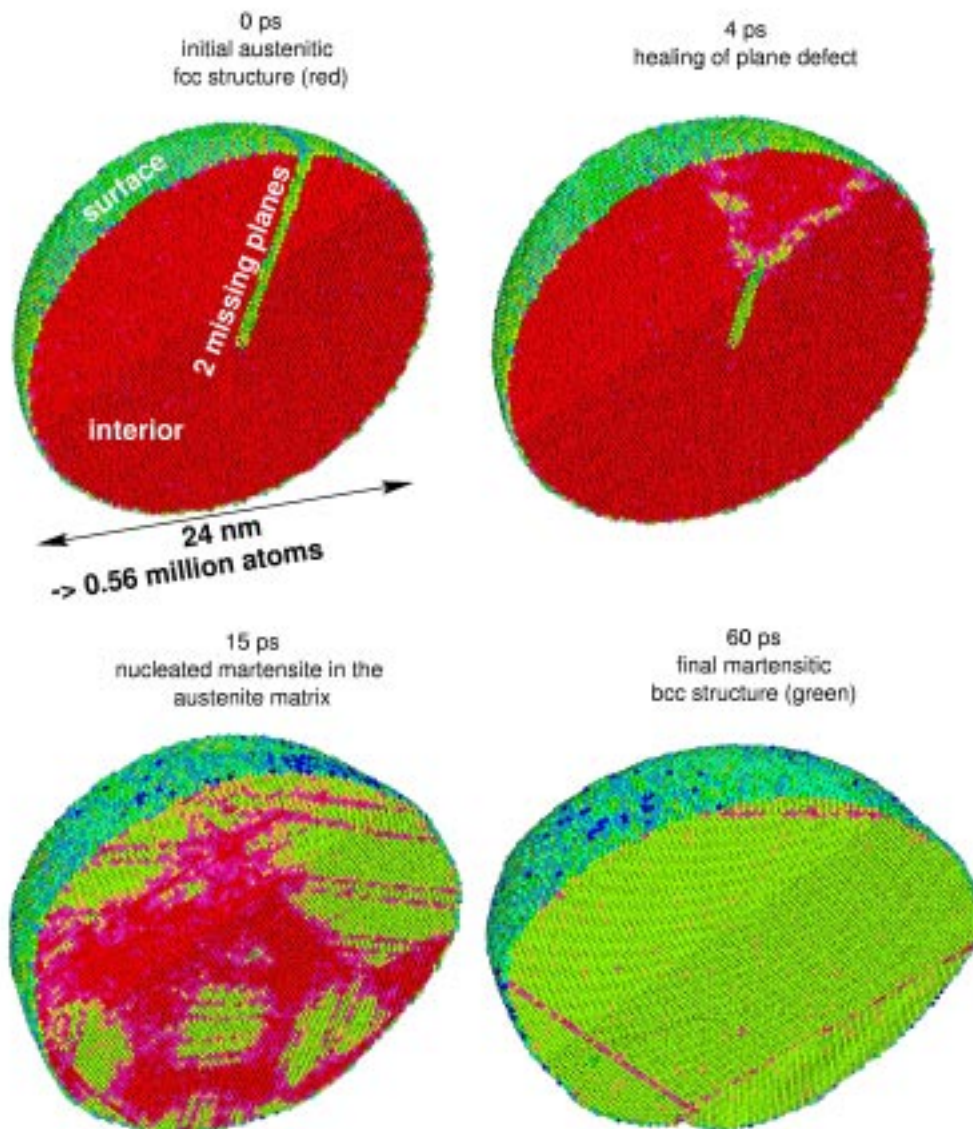


FIGURE 3

Nucleation of martensite (light atoms) at a plane defect in an otherwise ideal spherical $\text{Fe}_{80}\text{Ni}_{20}$ particle. The particle was initially prepared in the FCC structure (dark atoms). The intermediate structure at 50 K after 15 ps simulation time exhibits a pattern of differently oriented martensitic variants embedded in the austenitic structure. After 60 ps the particle has completely transformed to BCC and the plane defect has disappeared. Figure reprinted by permission from Taylor & Francis²².

The difficulty of the particles to undergo structural changes with decreasing temperature is connected with the energy barrier arising from the excess entropy of the high-temperature austenitic structure. In contrast, if spherical Fe–Ni particles free of defects are initially prepared in the BCC structure and then heated they transform spontaneously to the FCC phase, whereby the austenitic transformation temperature scales

with the inverse of the particle diameter as shown for a series of simulations in Fig. 4. This study reveals that the scaling is related to the variation of the difference of surface energies between the FCC and BCC phases¹⁶. Note that this scaling behavior resembles very much the variation of the melting temperature of the particles as a function of the inverse diameter (see below).

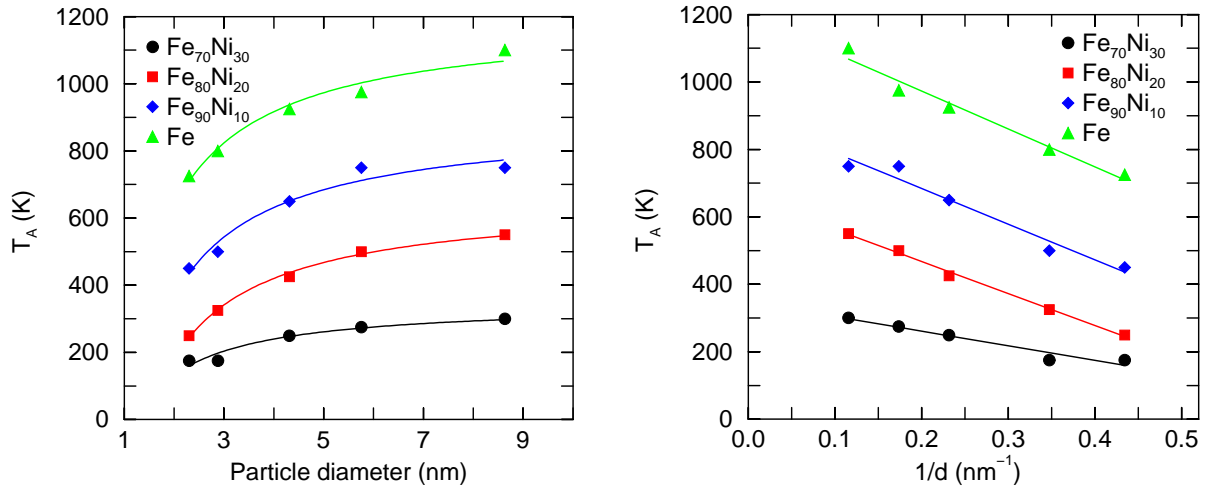


FIGURE 4

Variation of the austenitic transformation temperature T_A of Fe–Ni particles as a function of the cluster diameter d (left) and inverse cluster diameter (right)¹⁶. The extrapolation of $d \rightarrow \infty$ yields values for T_A lying within the range of experimentally observed values of A_S and A_F shown in Fig. 2.

We also have investigated nanophase Fe–Ni in the regime where softening with decreasing grain size occurs due to intergrain processes (anti Hall–Petch behavior). In this case the simulations show that the particles immediately attract each other, sinter and form grain boundaries, whereby the voids of the nanoparticle powder are unstable and gradually vanish within ns even without external pressure¹³. The volume of the resulting nanophase material after compaction is only slightly larger compared to the volume of the corresponding crystalline bulk material. Note that this kind of behavior (complete compaction if the initial average size of the particles is small enough) has been observed in molecular dynamics simulations of other nanophase materials like Cu²³. Calculation of the radial distribution function shows that when cooling the sintered Fe–Ni nanoparticles initially in the FCC structure, martensite easily grows from nucleation centers in the grain boundaries, however, the sample does not completely transform to BCC at low temperatures¹³.

Morphological transitions of sintered nanoparticles (in the gas phase or on a substrate) occur in simulations as well as in experiment and lead to icosahedral multiply twinned particles, which seem to be the lowest energy state for FCC particles with 4–7 nm

diameters^{24–26}. The instantaneous sintering of the particles leads first to crystalline-like surfaces of the initially spherical particles (even before the particles contact each other), which is the reason why the phenomenological law for the time two particles need to coalesce is not fulfilled^{27,28} ($\tau \propto r^4/(a^4\gamma D)$, where r is the cluster radius, a the atomic size, γ the surface energy and D the surface diffusion constant). Figure 5 exemplary shows the process of two-particle sintering with increasing temperature up to the melting point: A study by molecular dynamics simulations using embedded atom potentials.

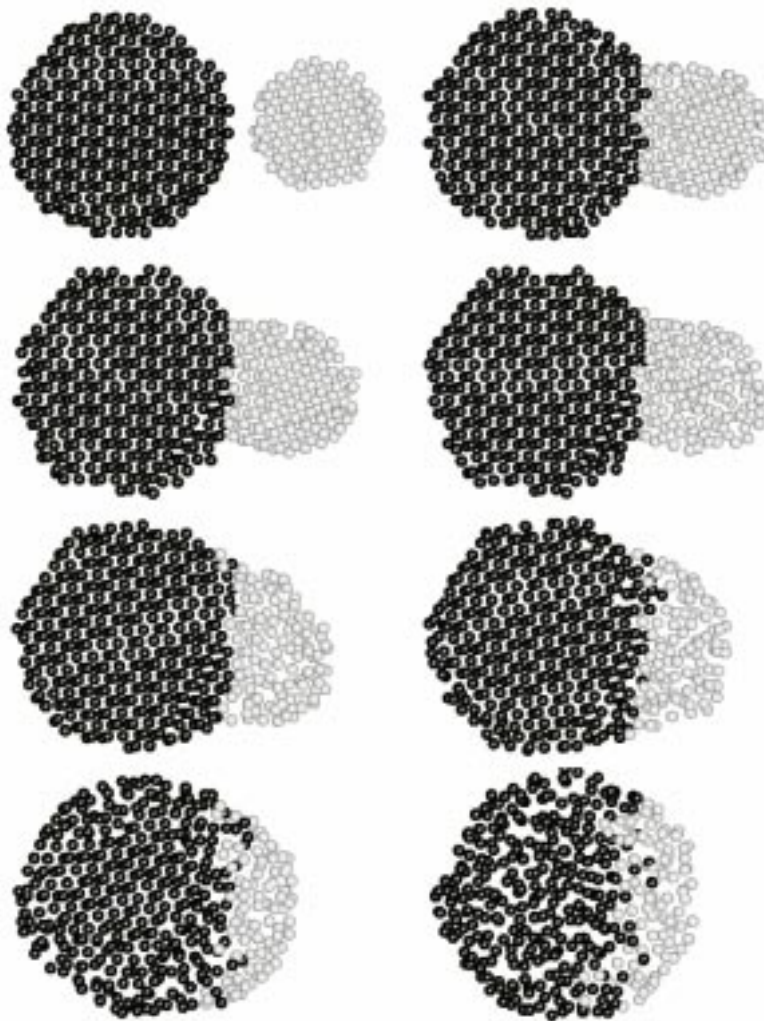


FIGURE 5

Sintering of two $\text{Fe}_{80}\text{Ni}_{20}$ particles of different sizes. After contact and neck formation at lower temperatures the smaller particle melts first and maximizes the contact. The Figure shows a cut through the spherical particles.

4. THE INFLUENCE OF MAGNETISM

So far in the simulations embedded atom potentials or other *semi-empirical* potentials have been used, in which the magnetic properties of the considered material enter only by the fit of the potential parameters to the elastic materials properties at low

temperatures. An explicit magnetic exchange interaction term is not considered. This means that the influence of magnetism on the martensitic transformation is not taken into account in an optimum way. In particular the influence of magnetic order is important if the Curie temperature becomes comparable to the martensitic/austenitic transformation temperature as it occurs in Fe–Pd, Ni–Mn–Ga *etc.* at appropriate compositions. This problem is complex in view of the different time scales of spin dynamics and atomic displacements and has so far not been solved in an optimum way. Model descriptions have been formulated to combine by Monte Carlo simulations the spin dynamics with updates of the volume with application to Fe–Ni nanoparticles²⁹. However, what is needed in addition, are electronic structure calculations of the clusters, i.e., handling the magnetic problem on an *ab initio* basis which is beyond the computer facilities available at present.

5. SIMILARITY OF STRUCTURAL TRANSFORMATION AND MELTING

We have investigated the melting of Fe, Ni, Fe–Ni and Al nanoparticles in a molecular dynamics study by using embedded atom potentials and tight-binding semi-empirical potentials. Here we concentrate on the melting and freezing of bulk Al and Al nanoparticles³⁰. While melting occurs without noticeable overheating, i.e., occurs spontaneously seemingly without any energy barrier involved, the melt can usually be undercooled. In the undercooled melt local structure elements develop having different symmetry than FCC, which is the symmetry of bulk Al.

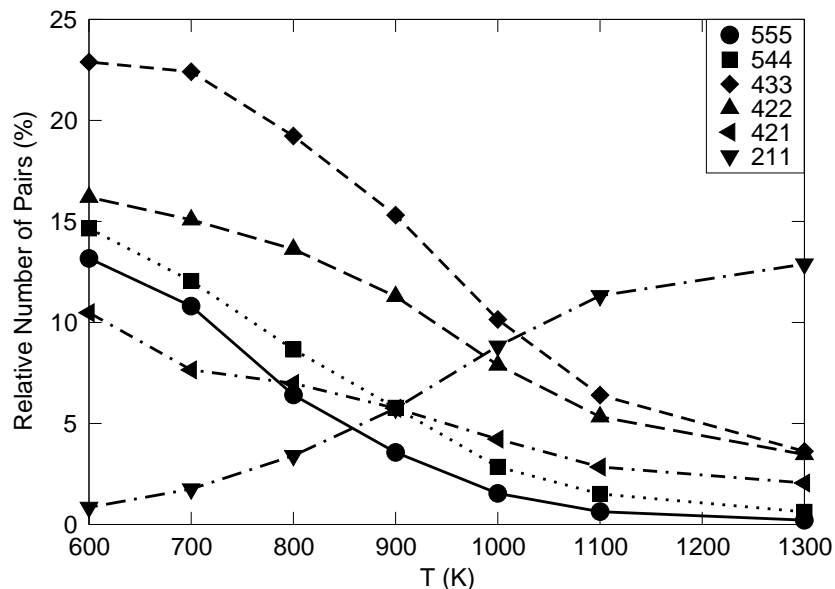


FIGURE 6

Common neighbor analysis of liquid Al showing the variation of the relative number of bonded pairs with common neighbor signatures for a given symmetry. For example, 421 and 422 denote FCC and HCP structures, respectively, while 555 characterizes an icosahedral element. Figure reprinted by permission from Taylor & Francis³⁰.

This can best be studied by calculating the radial distribution function $g_{lmn}(r)$, where the indices l, m, n allow a classification of the structure of the environment in which a given pair of atoms is embedded (*common neighbor analysis*)³⁰. The corresponding result for bulk Al is shown in Fig. 6. The results show that with decreasing temperature the abundance of structure elements with *wrong* symmetries increases. The local building blocks of icosahedral symmetry are directly responsible for the fact that metallic melts can be undercooled.

The melting of nanoparticles occurs spontaneously with increasing temperature similar to the melting of the bulk material, whereby the resulting structure of the liquid bears no resemblance to the crystalline structure of the solid nanoparticle, see Fig. 7 for the melting of an Al_{791} cluster. Figures 8 and 9 show the changes of the vibrational density of states and of the radial distribution function when passing from the liquid to the solid state.

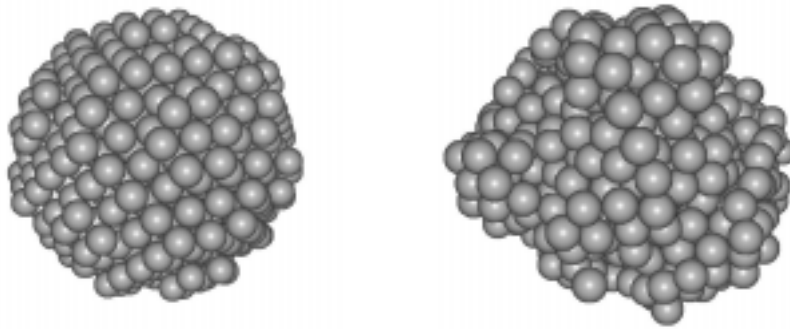


FIGURE 7

Solid (left) and liquid (right) phase of an Al particle containing 791 atoms at 300 K and 900 K, respectively.

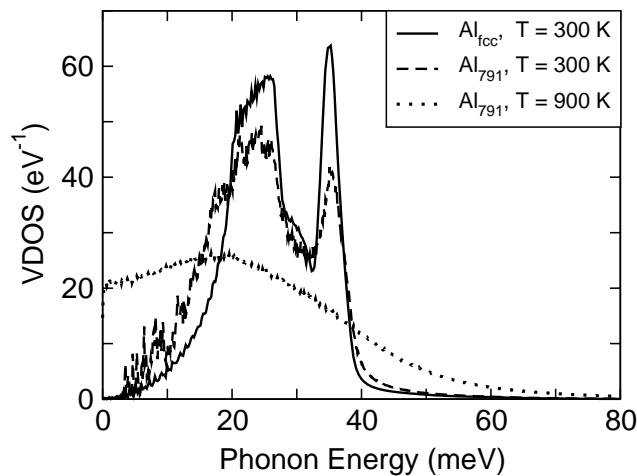


FIGURE 8

Vibrational density of states of solid and liquid Al_{791} compared to the bulk density of states (solid, dashed and dotted lines, respectively).

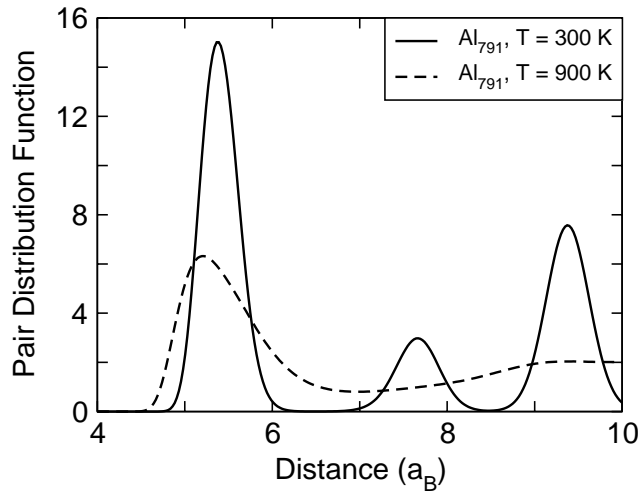


FIGURE 9

Radial distribution function of the Al_{791} particle in the solid and liquid phase as a function of the distance (in units of a_B). The function shows a first nearest neighbor peak in the liquid state but no marked peaks for the further neighbor shells indicating that the liquid nanoparticle has an amorphous-like structure.

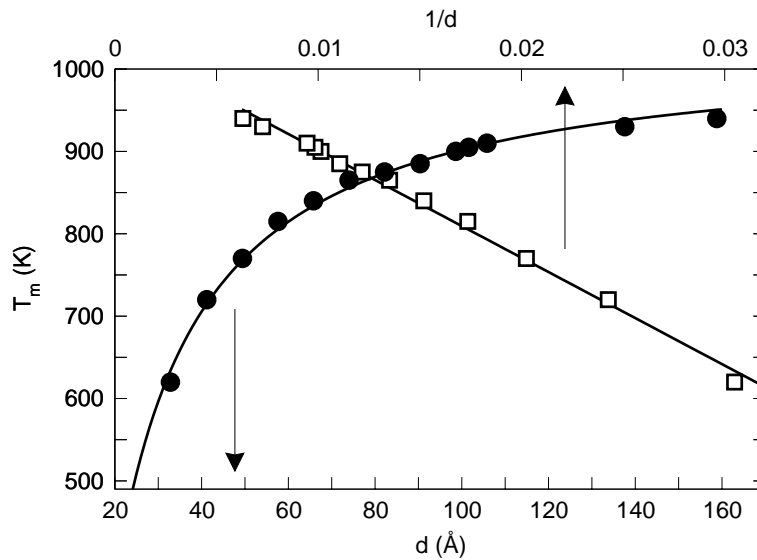


FIGURE 10

Melting temperature of free Al nanoparticles as a function of the diameter (filled circles) and reciprocal diameter (open squares).

Finally Fig. 10 shows the behavior of the melting temperature T_m as a function of the cluster diameter d : T_m scales with $1/d$ similar to the scaling behavior of the austenitic transition temperature.

When decreasing the temperature of the liquid Al or Ni nanoparticles freezing sets in at different temperatures depending on the history of the cooling process. The width of the hysteresis, shown in Fig. 11 for three different cases, in particular depends on the formation of local structure elements with icosahedral symmetry which survive in the

frozen nanoparticle and coexist with other symmetry elements leading to icosahedral multiply twinned nanoparticles as has been observed in the experiment²⁵.

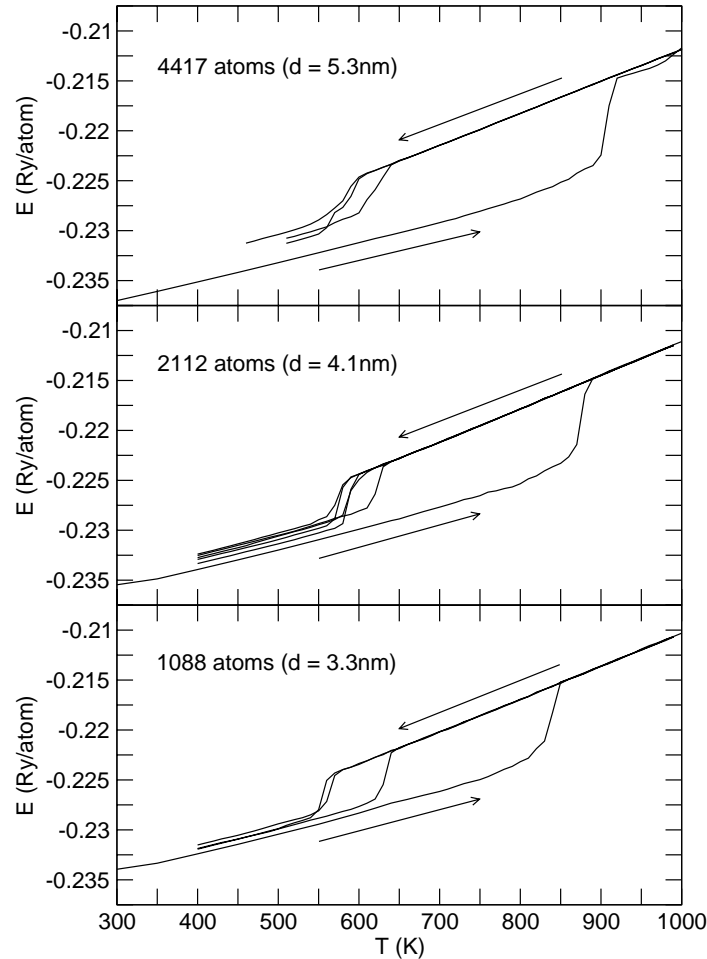


FIGURE 11

Hysteresis of melting/freezing of three Al nanoparticles with different sizes. The relatively sharp changes of the energy mark the transitions. The width of the hysteresis amounts to 260 K for the 3.3 nm particle, to 290 K for the 4.1 nm particle and to 320 K for the 5.3 nm particle.

6. CONCLUSIONS

We have discussed structural phase transformations and local symmetry changes in martensitic and liquid bulk systems and nanoparticles. While there is no universal behavior for the first order martensitic transformation or freezing of metallic melts, we observe universal behavior of the entropy driven austenitic and solid to liquid phase changes. In both cases the transition temperature scales with the reciprocal of the particle diameter. For the solid to liquid transition this behavior has theoretically been predicted some time ago³¹, experimental verification on Au nanoparticles has been achieved only recently³².

REFERENCES

- 1) P. LABASTIE, R.L. WHETTEN, *Phys. Rev. Lett.* **65**, 1567 (1990).
- 2) T. TADAKI, Y. MURAI, A. KOREEDA *et al.*, *Mater. Sci. Eng. A* **217–218**, 235 (1996).
- 3) I.M.L. BILLAS, A. CHÂTELAIN, W.A. DE HEER, *Science* **265**, 1682 (1994).
- 4) L. BLINOV, A. BUNE, P. DAWBEN *et al.*, *Phase Transitions* **77**, 161 (2004).
- 5) C.J. BRABEC, T. NANN, S.E. SHAHEEN, *MRS BULLETIN/JANUARY 2004*, 43.
- 6) R.E. CECH, D. TURNBULL, *Trans. AIME* **206**, 124 (1957).
- 7) R. MEYER, L.J. LEWIS, S. PRAKASH *et al.*, *Phys. Rev. B* **68**, 104303 (2003).
- 8) K. KADAU, T.C. GERMANN, P.S. LOMDAHL *et al.*, *Mater. Sci. Eng. A* (2004), in print.
- 9) J. SCHIØTZ, F.D.D. TOLLA, K.W. JACOBSEN, *Nature* **391**, 561 (1998).
- 10) R.W. SIEGEL, G.E. FOUGERE, Mechanical properties of nanophase materials, in: *Nanophase Materials – Synthesis – Properties – Applications*, eds. G.C. Hadjipanayis and R.W. Siegel, Vol. 260 of NATO ASI Series E, Kluwer, Dordrecht, The Netherlands 1990.
- 11) E.O. HALL, *Proc. Phys. Soc. (London) B* **64**, 747 (1951).
- 12) N.J. PETCH, *J. Iron Steel Inst.* **174**, 25 (1953).
- 13) K. KADAU, P. ENTEL, P.S. LOMDAHL, *Comp. Phys. Commun.* **147**, 126 (2002).
- 14) P. HAASEN, *Physical Metallurgy* (Cambridge University Press, U.K.).
- 15) R. MAEZAWA, S. KASHIMOTO, T. ISHIMASA, *Phil. Mag. Lett.* **84**, 215 (2004).
- 16) K. KADAU, M. GRUNER, P. ENTEL *et al.*, *Phase Transitions* **76**, 355 (2003).
- 17) P. ENTEL, R. MEYER, K. KADAU *et al.*, *Eur. Phys. J. B* **5**, 379 (1998).
- 18) M. MATSUMOTO, S. SAITO, I. OHMINE, *Nature* **416**, 409 (2002).
- 19) R. MEYER, P. ENTEL, *Phys. Rev. B* **57**, 5140 (1998).
- 20) K. KADAU, R. MEYER, P. ENTEL, *Surf. Rev. Lett.* **6**, 35 (1999).
- 21) <http://bifrost.lanl.gov/MD/MD.html>
- 22) K. KADAU, P. ENTEL, *Phase Transitions* **75**, 59 (2002).
- 23) H. ZHU, R.S. AVERBACK, *Mater. Sci. Eng. A* **204**, 96 (1995).
- 24) D.L. OLYNICK, J.M. GIBSON, R.S. AVERBACK, *Phil. Mag. A* **77**, 1205 (1998).
- 25) B. RELLINGHAUS, O. DMITRIEVA, S. STAPPERT, *J. Cryst. Growth* **262**, 612 (2004).
- 26) R. MEYER, J.J. GAFNER, S.L. GAFNER *et al.*, *Phase Transitions* (2004), submitted.
- 27) H. ZHU, R.S. AVERBACK, *Phil. Mag. Lett.* **73**, 27 (1996).
- 28) J.L. LEWIS, P. JENSEN, J.L. BARRAT, *Phys. Rev. B* **56**, 2248 (1997).
- 29) M.E. GRUNER, S. SIL, P. ENTEL, *Progr. Theor. Phys. Suppl.* **13**, 154 (2000).
- 30) M. KRETH, P. ENTEL, K. KADAU *et al.*, *Phase Transitions* **77**, 89 (2004).
- 31) P. PAWLOW, *Z. Phys. Chem.* **65**, 1 & 545 (1909).
- 32) P. BUFFAT, J.P. BOREL, *Phys. Rev. A* **13**, 2287 (1976).